Research article

Wenjing Yue, Song Gao, Yang Li*, Chunwei Zhang, Xiaoqian Fu and Duk-Yong Choi

Polarization-encrypted high-resolution full-color images exploiting hydrogenated amorphous silicon nanogratings

https://doi.org/10.1515/nanoph-2019-0500
Received December 3, 2019; revised January 22, 2020; accepted February 9, 2020

Abstract: As a prominent alternative to toxic dyes/pigments, nanostructural color pixels have garnered tremendous attention in applications related to display/imaging devices and color printings. However, current color pixels mostly offer static color responses. In relation to this, dynamic color tuning properties must be investigated in order to expand their functionalities and promote their use in the fields of encryption and anti-counterfeiting. In this study, a simple array of hydrogenated amorphous silicon nanogratings is proposed to realize polarization-encrypted full-color images via the coupling of incident light into different leaky mode resonances within the nanogratings. The proposed pixels can readily switch from vivid full colors to indistinguishable orange color by altering the incident polarization state. Hence, unlike the reported polarization-tuned color generation schemes that merely allow for the color variation of the image or require complicated designs to hide the color information, the proposed approach can encrypt arbitrary full-color images via a simple tuning of the incident polarization state. Owing to the localized leaky mode resonances supported by the nanogratings, the pixel can still implement the polarization-encrypted functionality even when it contains only four gratings, thus enabling a remarkably high resolution. The proposed simple scheme may provide a credible new pathway for accelerating the practical applications of high-resolution encryption and anti-counterfeiting.

Keywords: nanophotonics; structural color; encryption; polarization; leaky mode resonances.

1 Introduction

Metallic/dielectric nanostructures offer an effective way for manipulating light at the subwavelength scale by significantly enhancing the interaction with light over their bulk counterparts. Among the numerous studies on the interaction between light and nanostructures, one of the essential research topics discussed in recent decades is the structural color that can meet the growing number of applications, including high-resolution color printings [1–8], multi-function color display technologies [9, 10], colorful solar cells [11–13], colorimetric sensors [14–16] and multicolor meta-holograms [17–19], among others. Structural color inspired by nature originates from the wavelength-selective transmission, which is the absorption or reflection induced by the pre-designed nanostructures when the incident light impinges on them [20–22]. This physical structural color is a prominent alternative to toxic and carcinogenic dyes/pigments due to its conspicuous merits encompassing environment friendliness, high printing resolution, high reproduction fidelity and near-permanent non-fading performance. A number of representative configurations, such as periodically aligned nanoparticles/nanogratings [4–8, 23, 24] or multilayer thin films [10, 25–27] have been utilized to create structural colors by selectively enhancing or blocking the transmission/reflection at a specific resonant wavelength. However, the bottleneck of structural color generation lies

***Corresponding author: Yang Li,** School of Information Science and Engineering, University of Jinan, Jinan 250022, Shandong, China; and Shandong Provincial Key Laboratory of Network-based Intelligent Computing, University of Jinan, Jinan 250022, Shandong, China, e-mail: ise_liy@ujn.edu.cn. https://orcid.org/0000-0001-5260-5157
Wenjing Yue and Chunwei Zhang: School of Information Science and Engineering, University of Jinan, Jinan 250022, Shandong, China; and Shandong Provincial Key Laboratory of Network-based Intelligent Computing, University of Jinan, Jinan 250022, Shandong, China
Song Gao and Xiaoqian Fu: School of Information Science and Engineering, University of Jinan, Jinan 250022, Shandong, China
Duk-Yong Choi: Laser Physics Centre, Research School of Physics, Australian National University, Canberra, ACT 2601, Australia; and College of Information Science and Technology, Jinan University, Guangzhou, Guangdong 510632, China

in its static nature. In particular, once these structures are fabricated, their color information remains static and this can severely restrict their potential for future-oriented applications, such as security encryption, polarimetry microscopy, high-density optical data storage and active display technologies.

To this end, several schemes, including mechanical deformation [28, 29], liquid crystal-assisted optical systems [30, 31], metal/dielectric transitions via hydrogenation/dehydrogenation reaction [32, 33] and polarization-sensitive resonant structures [34–42], have been explored to implement advanced functionalities with dynamic color tunability. The design of a resonant structure featuring polarization-tuned spectra is regarded as a simple scheme to create dynamically alterable images. A periodical array of asymmetric structures, such as cross-shaped nanoantennas or nanoholes with different arm lengths [37, 39, 41], elliptical nanodisks [40] and one-dimensional (1D) nanogratings [34, 36, 38, 42] are intensively applied to realize polarization-dependent color responses. Compared with those two-dimensional nanostructures posing a great challenge in the fabrication process, 1D nanostructures are more suitable for the high-throughput fabrication and practical applications owing to the merits of ease of design and large-scale fabrications. The early scheme used to realize the polarization-tuned colors chiefly relies on the guided-mode resonance (GMR) [43]. This requires wavelength-comparable periodicity and sufficient unit cells to generate colors due to its grating coupling mechanism, thus limiting its applications in ultra-high-resolution display and imaging. Plasmonic structures based on the metallic nanostructures have been extensively used in the literature to achieve high-resolution color printing or imaging via the excitation of localized surface plasmonic resonance. However, as the metallic nanostructures are usually required to have a small size to achieve the excitation of resonance in the visible spectral regime, the fabrication of such fine metallic structures has a high requirement on the lithography technology. In addition, the reported resonant structures merely switch one specific color to a different one by altering the polarization state of the incident light [37–41]. In other words, the constructed color images only offer the dynamically variable colors but image information is unchangeable, thus limiting their applications in security encryption or anti-counterfeiting, which requires the structure to have the capability of encrypting the predefined color images.

In the current work, an approach for generating transmissive polarization-encrypted structural color is proposed and demonstrated by exploiting on hydrogenated amorphous silicon (a-Si:H) nanogratings (NGs). Silicon, as the most prevalent material in the semiconductor industry, has the salient advantages of ease of fabrication and is fully compatible with complementary metal-oxide-semiconductor process. Under the incident polarized illumination perpendicular to the nanograting orientation, the proposed color pixels offer bright and vivid full-color generation via a simple adjustment of the width of NGs. By switching the incident polarization state to be parallel to the NG axis, the pixels can render consistent orange color responses regardless of width variations in the NGs. We experimentally demonstrate the transition from the vivid and bright full colors to the identical orange color by altering the polarization state of the incident light. Further, the color image information embraced in a fabricated microscale color printing based on the a-Si:H NGs is verified to be successfully concealed by setting the incident illumination at the predesigned polarization state. Finally, the color pixels are theoretically and experimentally confirmed to be capable of the polarization-encrypted functionality even when the number of NGs in a pixel reduces to four, corresponding to a small pixel size of $1\,\mu m \times 1\,\mu m$. This result indicates that the proposed a-Si:H NGs-based color pixels open a new avenue for high-resolution encryption tag for security and anti-counterfeiting applications.

2 Results and discussion

Figure 1A depicts the concept of the proposed polarization-encrypted color pixels consisting of a periodically arranged 160 nm-thick a-Si:H NGs deposited on a glass substrate. The chosen a-Si:H is regarded as one of the best candidates for realizing transmission-type optical devices as it has relatively low loss and high refractive index in the visible wavelength regime compared with non-hydrogenated amorphous silicon (a-Si). For another common silicon material like crystalline silicon, even though it has a high refractive index in conjunction with lower optical loss, it faces huge difficulty in depositing on a glass substrate, which makes it unsuitable for transmission-type devices. The width and period of the a-Si:H NGs are denoted as W and P, respectively. Notably, the a-Si:H NGs used in the proposed pixel are typically small or comparable in size to the wavelength of interest, which is conducive to the realization of highly compact optical devices. The proposed color pixel can exhibit different color outputs under the orthogonal polarizations. For the transverse-electric (TE) polarized light that is perpendicular to the NG orientation, the transmissive color image is perceived by simply varying the width of the a-Si:H NGs. This color-rendering

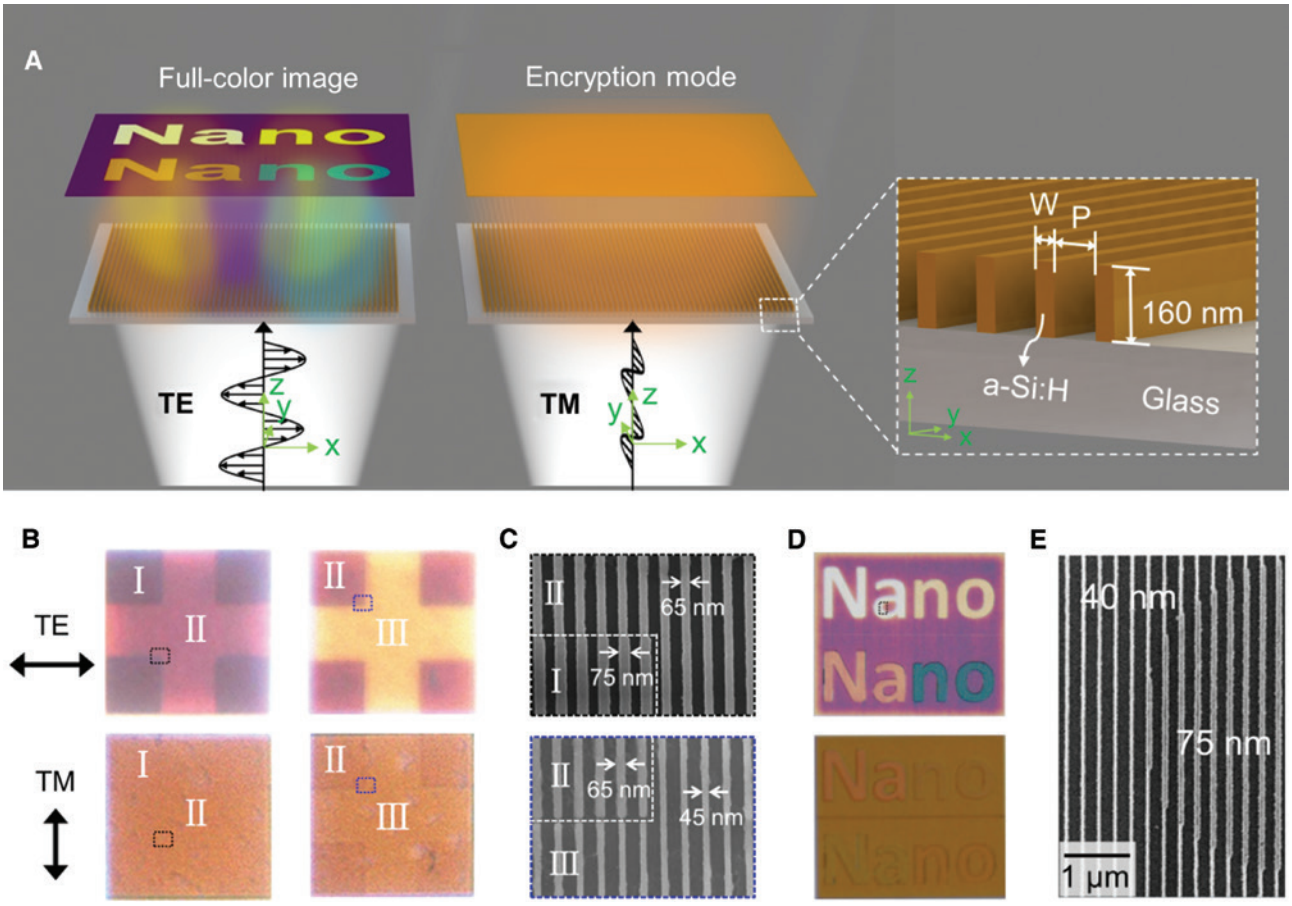

Figure 1: Concept and experimental demonstration of the proposed polarization-encrypted color pixels.
(A) The schematic of the proposed polarization-encrypted color pixels under the TE and TM polarized illuminations. The color pixels based on an array of a-Si:H NGs are capable of enabling full-color images under the TE polarized illumination and encrypting the image by rendering invariable orange color under the TM polarized illumination. The width and period of the NGs are denoted by W and P, respectively. The height of NGs is fixed at 160 nm. (B) The bright-field microscope images of the manufactured microscopic cross images (30 μm × 30 μm) under the TE and TM polarized illuminations. Regions of I, II and III represent the NGs with different widths of 75, 65 and 45 nm. (C) The corresponding SEM images at the corner of the cross, marked by the black and blue dotted boxes in (B). (D) Bright-field microscope images of the manufactured microscopic "NanoNano" images (100 μm × 85 μm) under the TE and TM polarized illuminations. (E) Corresponding SEM images of the region marked by the black dotted boxes in (D).

property is oriented from the scattering-induced strong leaky mode resonances within the a-Si:H NGs [44, 45]. Under the transverse-magnetic (TM) polarization with the E-field of the incident light parallel to the NG axis, the proposed pixels with different NG widths turn to encryption mode by offering stable output orange colors. This mode is different from the typical polarization-tuned schemes that generally provide two sets of variable color responses. This intriguing optical property may allow for the encryption of arbitrary full-color images, which can be intensively applied in practical applications, such as security tags and anti-counterfeiting coatings.

In an attempt to illustrate the proposed color rending scheme having feasibility for the application in security encryption, we demonstrate the complicated microscopic images that can switch from visible to invisible by altering the illuminated polarizations. Figure 1B shows 30 μm × 30 μm-sized cross images. Under the TE polarized light illumination, the microscopic color images clearly show vivid magenta and yellow cross patterns appearing in brilliant purple and magenta backgrounds, respectively. The distinct colors can be readily distinguished even at the corners and edges. Here, regions of I, II and III in the images exploit the NG widths of 75, 65 and 45 nm, respectively. As the incident light polarization switches to TM polarization, all the three regions of I, II and III show the same encrypted orange color. As such, the encrypted information recorded in the NGs (i.e. the cross pattern) becomes invisible. Figure 1C depicts the scanning electron microscope (SEM) images of the areas marked by the

black and blue dotted rectangular boxes in Figure 1B. The images reveal uniform line patterns and high fidelity of the fabricated devices. A more complicated and large-scale microscopic image containing "NanoNano", in which five distinct colors corresponding to the NG widths of 40, 45, 50, 75 and 90 nm are involved, is further demonstrated in Figure 1D. Likewise, the color information "NanoNano" is clearly seen under the TE polarized illumination and becomes invisible under the TM polarized illumination. Figure 1E exhibits the SEM images of the region marked by the black dotted rectangular box in Figure 1D. Based on the above observations, it is confirmed that the unique polarization-dependent characteristic of the proposed color pixels makes them suitable for security encryption and anti-counterfeiting applications.

To demonstrate a broad palette of transmissive colors, the pixels with a set of varied widths and periods were manufactured via a single-patterning process shown in Figure S1A. The process is further detailed in the experimental section. Figure S1B illustrates the SEM images of the manufactured color pixels, having NG widths of W = 50, 75 and 110 nm and constant period of P = 250 nm. Through the SEM images, it is clearly verified that the desired well-defined line pattern is attained. Figure 2A and B exhibis a polarization-switchable color palette comprising of 5 × 6 pixel arrays wherein each pixel has a dimension of 30 μm × 30 μm and features different NG widths and periods. Under the TE polarized illumination, the distinct color with high brightness and saturation is observed to be gradually tuned from yellow to magenta, and finally to cyan with increasing width from 40 to 110 nm, thus covering the entire visible spectral range. This result implies that the proposed scattering-mediated coloration approach implements a flexible broad color

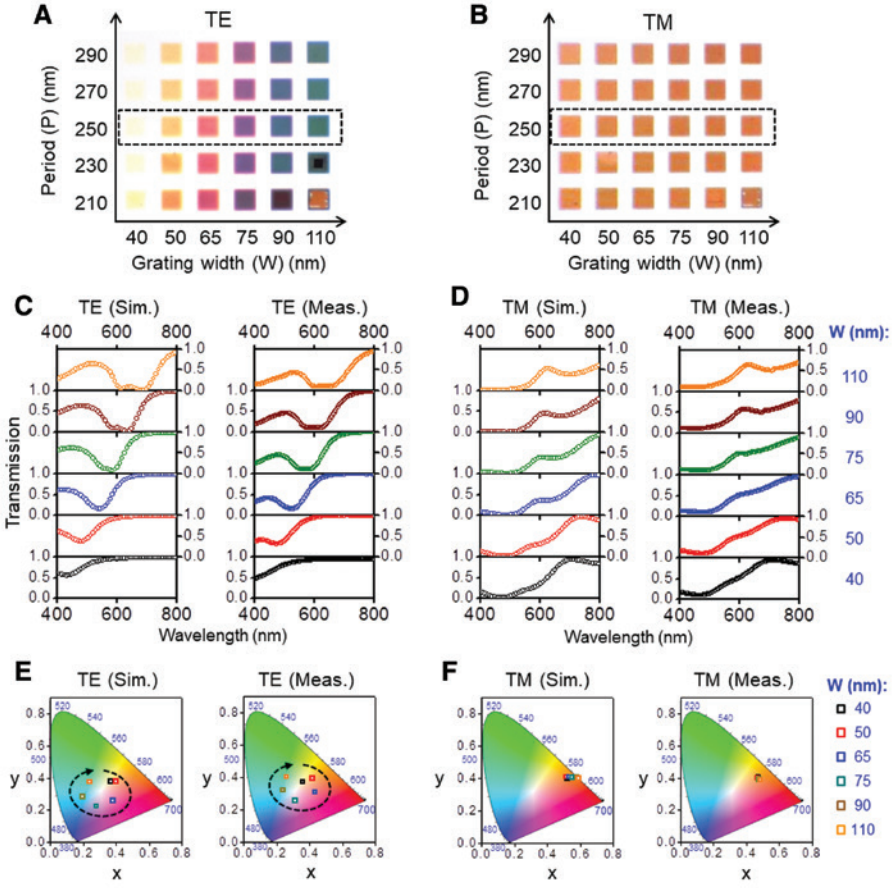

Figure 2: Simulated and measured optical performances of the proposed color pixels.
The bright-field microscopy images of the manufactured color palette with the stepwise tuning of W and P under the (A) TE and (B) TM polarized illuminations. Each pixel belonging to the color palette has a footprint of 30 μm × 30 μm. Simulated and measured transmission spectra for the pixels, marked by a dotted box in 2(A) and 2(B), under the (C) TE and (D) TM polarized illuminations. The corresponding chromaticity coordinates of the color pixels in the CIE 1931 chromaticity diagram for the (E) TE and (F) TM polarizations.

tuning property depending on the width of NGs. In contrast to the full-color generation under the TE polarized illumination, all the manufactured pixels exhibit indistinguishable orange colors with similar levels of color saturation and brightness under the TM polarized illumination, as depicted in Figure 2B, reasonably confirming the proposed polarization-encrypted concept. For a constant NG width, the color hardly changes with the array period varying from 210 to 290 nm for both TE and TM polarizations. This finding indicates that there is no diffraction effect in such a periodical NG array; thus, the near-field coupling effect between two NGs can be neglected. Figure S2 displays the dependence of the transmission spectra of the pixels with different NG widths upon the periods under the TE and TM polarized illuminations, respectively. Notably, the transmission spectra under both TE and TM polarized illuminations approximately maintain invariable in terms of the resonance wavelength, spectral bandwidth and efficiency at off-resonance as the period is changed.

To further explore the polarization-enabled tunable functionality of the proposed scheme, the transmission spectra under the TE and TM polarized light illuminations are systematically investigated as a function of the width of a-Si:H NGs at a fixed period of P = 250 nm. As plotted in Figure 2C, the measured spectra exhibit a good match with the simulated ones in terms of their resonance wavelengths and the overall spectral profiles. The obtained transmission spectra for TE polarization are characterized by a strong suppression at resonance and remarkably high transmission efficiency of ~90% at the off-resonance of the long-wavelength side. At off-resonance of the short-wavelength side, the transmission efficiency is relatively low due to the inevitable optical loss of a-Si:H. In the simulation, ~50% efficiency can be obtained, whereas in the measurement, lower efficiency is attained, especially for the pixels with larger NG width.

Figure S3 shows the simulated transmission spectra of the proposed a-Si:H NGs-based pixels in comparison to that of the non-hydrogenated a-Si NGs. As can be seen, the proposed a-Si:H NGs-based pixels offer better transmission spectra with higher transmission efficiency at off-resonance in conjunction with larger suppression ratio. With the width of NGs increasing from 40 to 110 nm, the resonance wavelength gradually redshifts from 440 to 670 nm, in correspondence to the observed vivid color images marked by the black dotted box in Figure 2A. Figure 2D presents the well-matched simulated and measured transmission spectra under the TM polarized illumination. As the width of NGs ranges from W = 40 to 110 nm, the proposed pixels offer unaltered transmission spectra with the efficiency close to zero in the short wavelength spectral range (<500 nm) and slightly increasing with the wavelength exceeding 500 nm. The relevant chromaticity coordinates are calculated based on the simulated and measured transmission spectra and then plotted in the International Commission on illumination (CIE) 1931 chromaticity diagram. By augmenting the width of NGs, the chromaticity coordinates for the TE polarization, as depicted in Figure 2E, are observed to evolve along the black arrow and form a circle, thereby suggesting the capability for full-color production by applying this approach. For the TM polarization, the calculated color coordinates indicate the stable orange color response in both theory and experiment, which is in accordance with the observed orange colors in Figure 2B. Notably, the experimental observations are more superior to the simulated ones in terms of the consistency of the saturation of output color, which is more propitious to hide the information. In addition, the dependence of the thickness of NG on the simulated transmission spectra and the chromaticity coordinates of color pixels are also investigated and presented in Figure S4A and S4B, respectively. Here, we consider three pixels having NG widths of 90, 65 and 50 nm, which correspond to the primary subtractive colors of cyan, magenta and yellow (CMY). Under the TE polarized illumination, the yellow and magenta pixels have nearly unalterable resonance wavelengths but gradually increasing suppression in transmission when the NG thickness varies from 50 to 250 nm. As the transmission spectrum with high suppression ratio corresponds to high color saturation, the NG thickness is preferred to exceed around 150 nm. While for the cyan pixel under the TE polarized illumination, it can be observed that the NG thickness should be set at around 160 nm to maintain the highly saturated cyan color. For the TM polarization, CMY pixels feature analogous transmission spectra. To obtain similar color responses for the encryption mode, the NG thickness should be larger than 160 nm. Moreover, NG with high aspect ratio can impose difficulties in fabrication, especially for the yellow pixel that has a narrow NG width. Therefore, the thickness of NG of the proposed pixels is properly set as 160 nm.

Unlike the extensively studied dielectric diffraction gratings and photonic crystals, which generate colors due to periodic index modulations and rely on long-range order, the individual a-Si:H NG in the array excites a localized leaky optical mode resonance within the NG via a strong scattering property owing to the high refractive index of a-Si:H [44–46]. As the proposed pixels have a small grating period of 250 nm compared to the visible wavelengths, sufficiently low filling factors and small grating thickness, both high-order diffraction and GMR effects are effectively avoided in our proposed 1D NGs

[45]. When the incident light is coupled into different NGs' leaky mode resonances under the TE and TM illuminated polarizations, the generated colors of the NG exhibit strong polarization dependence.

In an effort to verify the leaky optical modes supported by the proposed pixels, the transmission spectra and corresponding intensity distributions of electric (E) field and magnetic (H) field at resonance are meticulously inspected, as noted in Figure 3. When the incident light wavelength matches with the optical mode resonance supported by the NG, strong enhancement of the field intensities can be observed. Figure 3A and B plot the simulated transmission spectra of CMY pixels under the TE and TM polarized illuminations, respectively. Under the TE polarized illumination, the pixels with smaller widths of W = 50 and 65 nm have single resonance dips at the wavelengths of 483 and 541 nm, respectively. For the pixel with wider width of W = 90 nm, two closely neighboring resonance dips are observed to exist at the wavelengths of 582 and 633 nm, respectively. Figure 3C illustrates the intensity profiles of H-field ($|H|^2$) at these resonance wavelengths. At the resonance wavelengths of 483, 541 and 633 nm, a strong intensity enhancement of the H-field can be observed within the a-Si:H NG, as shown in Figure 3C (i, ii, iv), thus verifying the presence of the TE_{01} leaky mode resonance supported by the NG. Different from the observed single field intensity maxima, two intensity maxima, as shown in Figure 3C (iii), appear within the a-Si:H NG at the resonance wavelength of 582 nm, similar to the TE_{11} leaky mode resonance. Under the TM polarized illumination, the pixels generate prime transmission peaks in the near-infrared wavelength region, as shown in Figure 3B. At the visible wavelength range, the spectra maintain similar profiles overall. Figure 3D (i, ii, iii) depicts the intensity profiles of the E-field ($|E|^2$) at the resonance wavelengths of 723, 773 and 845 nm, respectively, which are associated with the primary transmission peaks for the pixels with the corresponding widths of 50, 65 and 90 nm. Two intensity maxima observed inside a-Si:H NG indicate that the TM_{11} leaky mode resonances are excited.

As the individual a-Si:H NG can excite the resonance mode, a single NG is envisioned to be capable of creating a specific color in theory. Nevertheless, the resonance supported by the single NG is usually not strong enough to realize the desired high-saturation output colors. Figure 4A and B show the simulated

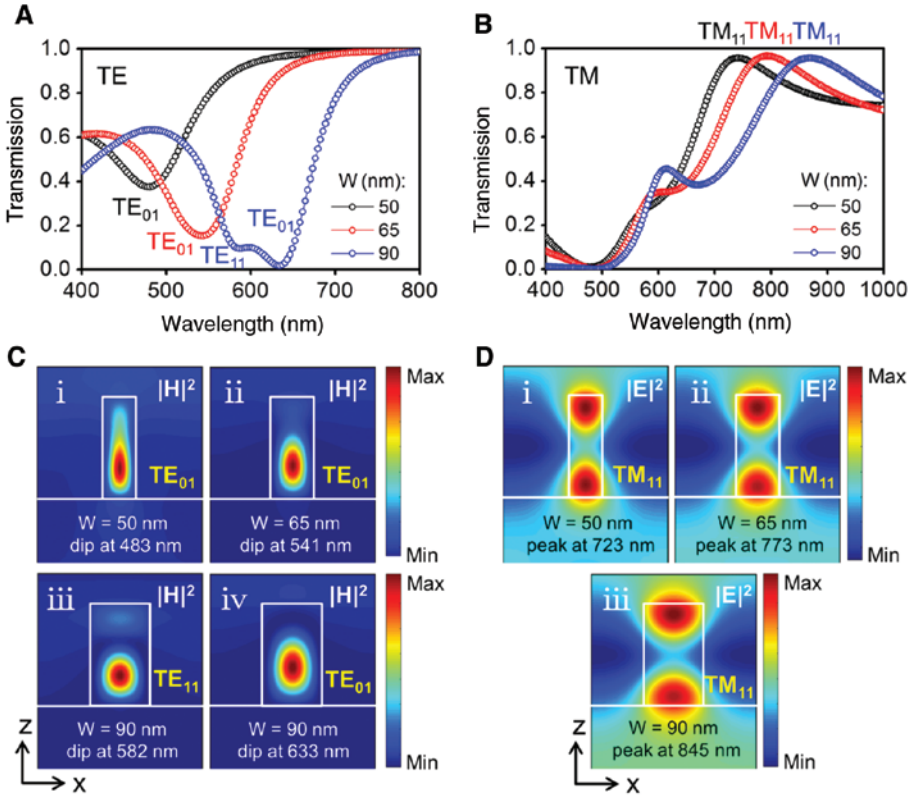

Figure 3: Resonance modes excited by the proposed color pixels.
The simulated transmission spectra of the pixels with widths of 50, 65 and 90 nm under the (A) TE and (B) TM polarized illuminations. Intensity profiles of (C) H- and (D) E-field ($|H|^2$, $|E|^2$) at the resonant wavelengths under the TE and TM polarized light.

polarization-dependent transmission spectra for the CMY pixels with changing the number of NGs. Under the TE polarized illumination, the spectra tend to exhibit an acceptable resonance dip when the numbers of NGs increase to three, with merely scarifying a small portion of transmission efficiency at off-resonance, as evidenced by Figure 4A. Hence, as plotted in Figure S5A, the CMY pixels based on three NGs can still generate color responses with reasonably good saturation levels, which are the same as the pixels based on the infinite NGs. Noting that the overall spectral profiles and the color responses under the TE polarized illumination are not dramatically altered and retain similarities to a certain extent. Figures 4B and S5B present the dependence of the transmission spectra and color coordinates under the TM polarized illumination on the number of NGs, where both the spectra and color responses are observed to be acutely changed. Despite all these, as the number of NGs increases from 1 to 4, the transmission spectra gradually evolve to the expected spectra provided by an infinite number of NGs. Based on the color coordinates in the CIE chromaticity diagram, the uniform orange colors are perceived for the CMY pixels comprising only four NGs, corresponding to an ultra-compact dimension of 1 μm × 1 μm. To experimentally verify the above observation, we prepare five samples composed of four color pixels with different dimensions (10 μm × 10 μm, 5 μm × 5 μm, 2 μm × 2 μm, 1 μm × 1 μm and 0.5 μm × 0.5 μm, respectively), as presented in Figure 4C. According to the SEM image taken from the sample with the pixel dimension of 1 μm × 1 μm, it can be clearly seen that the pixel in the top right corner contains four NGs. From the optical microscope images, it is verified that even when the color pixel dimension reduces to 1 μm × 1 μm, four distinct colors can be easily perceived under the TE polarized illumination, while indistinguishable orange colors are generated from all the color pixels under the TM polarized

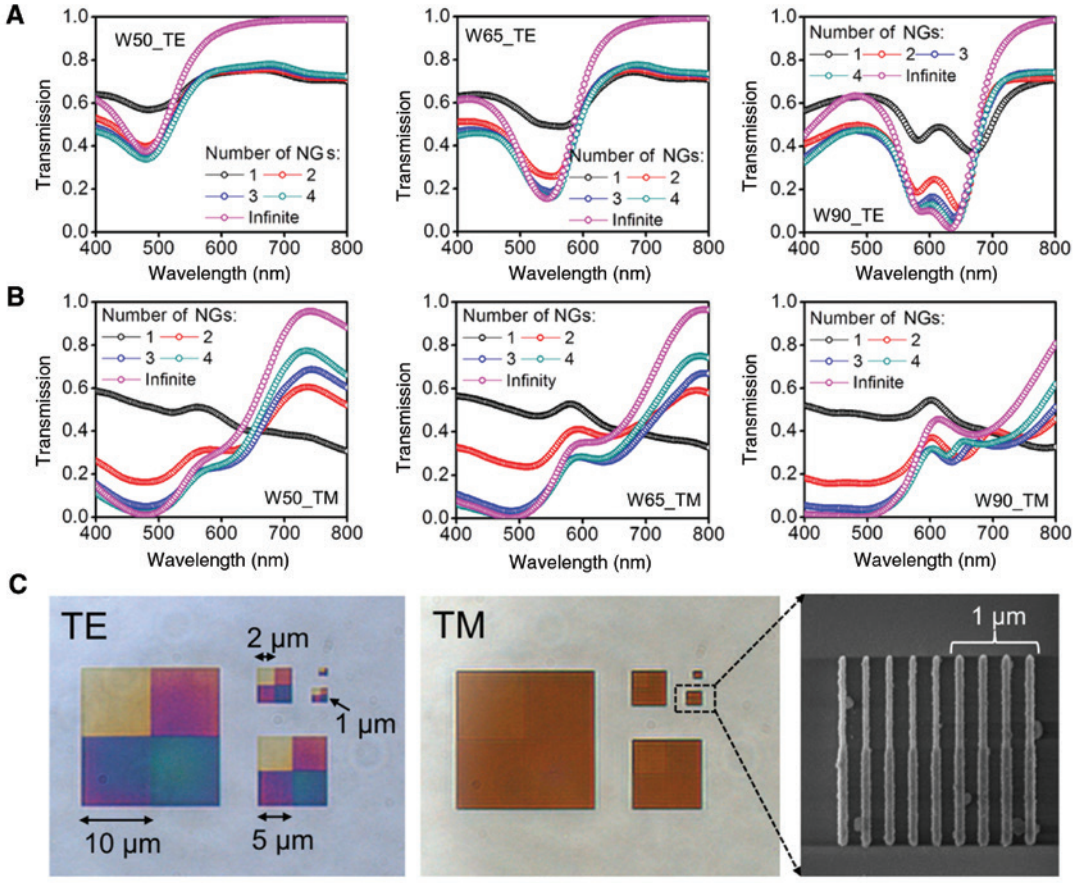

Figure 4: Realized high resolution of the proposed color pixels.
The dependence of the simulated transmission spectra of the pixels with different NG widths of 50, 65 and 90 nm on the number of NGs under the (A) TE and (B) TM polarized illuminations. (C) The bright-field microscope images of the prepared samples having different pixel dimensions (10 μm × 10 μm, 5 μm × 5 μm, 2 μm × 2 μm, 1 μm × 1 μm and 0.5 μm × 0.5 μm). The SEM image taken from the sample with the pixel dimension of 1 μm × 1 μm is given on the right.

illumination. In conclusion, the proposed polarization-encrypted concept can function well even when the pixel dimension downscales to 1 μm × 1 μm corresponding to a high spatial resolution of ~25,400 dpi. This finding indicates that the proposed color pixels have potentials in the fields of high-resolution display/image devices and information encryption. Moreover, even though the achieved resolution here is not comparable to that of the previously reported nanodisk-enabled color printings [4–8, 47], it is much higher than the previously demonstrated 1D gratings-based polarization-encrypted approaches [34, 36, 42, 43], which require wavelength-comparable periodicity and sufficient unit cells to generate polarization-dependent colors. From another perspective, the achieved high resolution also validates that the proposed 1D a-Si:H NG array is predominantly induced by the localized leaky resonances as stated in the previous section, rather than the common GMR effect residing in the subwavelength gratings.

Another major attraction of the proposed a-Si:H NGs-based color pixels is the angular tolerant property, which is superior to the previously reported GMR-mediated approaches that exhibit a strong dependence of the color response on the periodicity. The non-iridescent structural colors for wide viewing angles provided by the proposed pixels also arise from the excitation of the highly localized resonance mode within NGs, which is predominantly dependent on the width of NGs rather than the array period. To verify the angle-insensitive property, the angle-resolved transmission spectra of the proposed pixels with NG widths of D = 50, 65 and 90 nm are respectively examined under the TE and TM polarized light illuminations, as illustrated in Figure S6. As can be clearly seen, the resonant wavelength and the overall shape of the transmission spectra remain almost constant over a wide range of incident angles up to 30°, thus indicating the relaxed angular tolerance.

3 Conclusion

In summary, we have proposed and demonstrated polarization-encrypted structural colors by exploiting a simple array of a-Si:H NGs. Depending on the polarization state, the incident light is coupled to different leaky optical mode resonances within the NGs. Under the TE polarized illumination, the resonances occur in the visible spectral regime and can be tuned by altering the width of NGs, eventually generating the highly saturated full colors. When the polarization state switches to the TM mode, the indistinguishable orange color is rendered regardless of the variation of the NG width as the main resonance modes supported by the NGs appear in the infrared spectral region. As proof of the claimed encryption concept, microscopic color images containing cross patterns and "NanoNano" information were respectively prepared by fixing the widths of NG at different values. Results indicated that the color information can be successfully concealed via the simple polarization tuning from TE to TM. In addition, the proposed color pixels are established to retain the polarization-encrypted functionality even when their dimensions downscale to 1 μm × 1 μm, which merely contains four NGs. The presented strategy facilitates the development and the practical use of high-resolution multi-functional display, security tag, and anti-counterfeiting.

4 Experimental section

4.1 Device fabrication

The proposed a-Si:H NGs were fabricated by adopting a series of standard processes, including chemical vapor deposition, electron beam lithography (EBL) and plasma dry etching. A 160 nm-thick a-Si:H film was initially deposited on a glass substrate by virtue of a gas mixture of SiH_4 (silane) and helium carrier via plasma enhanced chemical vapor deposition (PECVD) (Oxford, Plasmalab System 100). A film made of a positive electron beam resist of ZEP520A was subsequently patterned with the EBL system (RAITH 150), and then dry-etched through a plasma etcher (Oxford, Plasmalab System 100) using a gas mixture of CHF_3 and SF_6. The residual resist was removed by oxygen plasma in the etcher. The completed color pixels exhibit dimensions of 30 μm × 30 μm.

4.2 Optical characterization and simulation

The prepared color pixels were visually scrutinized under a high-resolution field emission scanning electron microscope (Hitachi, Regulus-8100). The transmission microscopic images related to each pixel in Figure 1B and D, Figure 2A and B and Figure 4C were captured under normal incidence using a digital microscope (Leica, DM4000M). The transmission microscopic images in Figure 1B and D, Figure 2A and B and Figure 4C are measured through 20×, 50×, 100× objective lens, respectively. The optical transmission spectra for TE and TM polarizations were

measured under normal incidence using a commercial microspectrophotometer (Craic, 20/30PV), which had the capability to measure the polarization-dependent transmission spectra in a micro area in the spectral regime from 200 to 2100 nm. Here, linear polarized light with a spot size of 10 μm was applied to measure the transmission spectra of the manufactured color pixels (30 μm × 30 μm) in Figured 2C and 2D. A commercial tool based on the finite difference time domain (FDTD) method (Lumerical, FDTD Solutions) was utilized in order to explore the polarization-dependent transmission spectra at normal incidence, angle-resolved transmission spectra, and intensity distributions of E- and H-field. The refractive index of a-Si:H used in the simulation, as plotted in Figure S7, was measured by a reflecto-spectrometer (Scientific Computing International, Filmtek 4000), which operated in the spectral regime from 450 to 1650 nm. The Filmtek 4000 measuring system employed the Scientific Computing International company's generalized material model with advanced global optimization algorithms for high-precision refractive index measurement. By using Filmtek 4000, two spectroscopic reflection data were gathered from the a-Si:H film on the glass substrate at normal and 70° incidences. These two reflection data were then fitted with the material model to derive the complex refractive index of a-Si:H. The complex refractive index of the non-hydrogenated a-Si originated from Palik [48].

Acknowledgments: This work was supported by the National Natural Science Foundation of China (NSFC) (Grant Nos. 61805101 and 61604060), the Natural Science Foundation of Shandong Province (Grant Nos. ZR2019BF013, ZR2017JL027, ZR2018BF025, Funder Id: http://dx.doi.org/10.13039/501100007129), and by the China Postdoctoral Science Foundation (Grant No. 2018M632605). This work was performed in part at the ACT node of the Australian National Fabrication Facility, a company established under the National Collaborative Research Infrastructure Strategy to provide nano and micro-fabrication facilities for Australia's researchers.

References

[1] Ji C, Lee KT, Xu T, Zhou J, Park HJ, Guo LJ. Engineering light at the nanoscale: structural color filters and broadband perfect absorbers. Adv Opt Mater 2017;5:1700368.
[2] Kristensen A, Yang JKW, Bozhevolnyi SI, et al. Plasmonic colour generation. Nat Rev Mater 2016;2:16088.
[3] Gu Y, Zhang L, Yang JKW, Yeo SP, Qiu CW. Color generation via subwavelength plasmonic nanostructures. Nanoscale 2015;7:6409–19.
[4] Zhu X, Yan W, Levy U, Mortensen NA, Kristensen A. Resonant laser printing of structural colors on high-index dielectric metasurfaces. Sci Adv 2017;3:e1602487.
[5] Sun S, Zhou Z, Zhang C, et al. All-dielectric full-color printing with TiO metasurfaces. ACS nano 2017;11:4445–52.
[6] Zhu X, Vannahme C, Hojlund-Nielsen E, Mortensen NA, Kristensen A. Plasmonic colour laser printing. Nat Nanotechnol 2016;11:325–9.
[7] Miyata M, Hatada H, Takahara J. Full-color subwavelength printing with gap-plasmonic optical antennas. Nano Lett 2016;16:3166–72.
[8] Kumar K, Duan H, Hegde RS, Koh SCW, Wei JN, Yang JKW. Printing colour at the optical diffraction limit. Nat Nanotechnol 2012;7:557–61.
[9] Ge D, Lee E, Yang L, et al. A robust smart window: reversibly switching from high transparency to angle-independent structural color display. Adv Mater 2015;27:2489–95.
[10] Guo J, Huard CM, Yang Y, Shin YJ, Lee KT, Guo LJ. ITO-free, compact, color liquid crystal devices using integrated structural color filters and graphene electrodes. Adv Opt Mater 2014;2:435–41.
[11] Soman A, Antony A. Colored solar cells with spectrally selective photonic crystal reflectors for application in building integrated photovoltaics. Sol Energy 2019;181:1–8.
[12] Peharz G, Berger K, Kubicek B, et al. Application of plasmonic coloring for making building integrated PV modules comprising of green solar cells. Renew Energy 2017;109:542–50.
[13] Zhang W, Anaya M, Lozano G, et al. Highly efficient perovskite solar cells with tunable structural color. Nano Lett 2015;15:1698–702.
[14] Kou D, Ma W, Zhang S, Lutkenhaus JL, Tang B. High-performance and multifunctional colorimetric humidity sensors based on mesoporous photonic crystals and nanogels. ACS Appl Mater Interfaces 2018;10:41645–54.
[15] Moirangthem M, Arts R, Merkx M, Schenning APHJ. An optical sensor based on a photonic polymer film to detect calcium in serum. Adv Funct Mater 2016;26:1154–60.
[16] Choi SY, Mamak M, von Freymann G, Chopra N, Ozin GA. Mesoporous bragg stack color tunable sensors. Nano Lett 2006;6:2456–61.
[17] Li X, Chen L, Li Y, et al. Multicolor 3D meta-holography by broadband plasmonic modulation. Sci Adv 2016;2:e1601102.
[18] Huang K, Dong Z, Mei S, et al. Silicon multi-meta-holograms for the broadband visible light. Laser Photonics Rev 2016;10:500–9.
[19] Huang YW, Chen WT, Tsai WY, et al. Aluminum plasmonic multicolor meta-hologram. Nano Lett 2015;15:3122–7.
[20] Lopez-Garcia M, Masters N, O'Brien HE, et al. Light-induced dynamic structural color by intracellular 3D photonic crystals in brown algae. Sci Adv 2018;4:eaan8917.
[21] Vukusic P, Sambles JR. Photonic structures in biology. Nature 2003;424:852–5.
[22] Vukusic P, Sambles JR, Lawrence CR. Colour mixing in wing scales of a butterfly. Nature 2000;404:457–7.
[23] Yue W, Gao S, Lee SS, Kim ES, Choi DY. Highly reflective subtractive color filters capitalizing on a silicon metasurface integrated with nanostructured aluminum mirrors. Laser Photonics Rev 2017;11:1600285.
[24] Lee KT, Jang JY, Park SJ, et al. Subwavelength nanocavity for flexible structural transmissive color generation with a wide viewing angle. Optica 2016;3:1489–95.

[25] Kats MA, Blanchard R, Genevet P, Capasso F. Nanometre optical coatings based on strong interference effects in highly absorbing media. Nat. Mater. 2012;12:20–4.
[26] Li Z, Butun S, Aydin K. Large-area, lithography-free super absorbers and color filters at visible frequencies using ultrathin metallic films. ACS Photonics 2015;2:183–8.
[27] Park CS, Shrestha VR, Lee SS, Kim ES, Choi DY. Omnidirectional color filters capitalizing on a nano-resonator of Ag-TiO_2-Ag integrated with a phase compensating dielectric overlay. Sci Rep 2015;5:8467.
[28] Tseng ML, Yang J, Semmlinger M, Zhang C, Nordlander P, Halas NJ. Two-dimensional active tuning of an aluminum plasmonic array for full-spectrum response. Nano Lett 2017;17:6034–9.
[29] Song S, Ma X, Pu M, et al. Actively tunable structural color rendering with tensile substrate. Adv Opt Mater 2017;5:1600829.
[30] Olson J, Manjavacas A, Basu T, et al. High chromaticity aluminum plasmonic pixels for active liquid crystal displays. ACS nano 2016;10:1108–17.
[31] Franklin D, Chen Y, Vazquez-Guardado A, et al. Polarization-independent actively tunable colour generation on imprinted plasmonic surfaces. Nat Commun 2015;6:7337.
[32] Duan X, Liu N. Scanning plasmonic color display. ACS Nano 2018;12:8817–23.
[33] Duan X, Kamin S, Liu N. Dynamic plasmonic colour display. Nat Commun 2017;8:14606.
[34] Wu S, Ye Y, Duan H, Gu Y, Chen L. Large-area, optical variable-color metasurfaces based on pixelated plasmonic nanogratings. Adv Opt Mater 2019;7:1801302.
[35] Jang J, Jeong H, Hu G, Qiu CW, Nam KT, Rho J. Kerker-conditioned dynamic cryptographic nanoprints. Adv Opt Mater 2019;7:1801070.
[36] Finlayson ED, Hooper IR, Lawrence CR, et al. Covert images using surface plasmon-mediated optical polarization conversion. Adv Opt Mater 2018;6:1700843.
[37] Heydari E, Sperling JR, Neale SL, Clark AW. Plasmonic color filters as dual-state nanopixels for high-density microimage encoding. Adv Funct Mater 2017;27:1701866.
[38] Yue W, Lee SS, Kim ES. Angle-tolerant polarization-tuned color filter exploiting a nanostructured cavity. Opt Express 2016;24:17115–24.
[39] Li Z, Clark AW, Cooper JM. Dual color plasmonic pixels create a polarization controlled nano color palette. ACS Nano 2016;10:492–8.
[40] Goh XM, Zheng Y, Tan SJ, et al. Three-dimensional plasmonic stereoscopic prints in full colour. Nat Commun 2014;5:5361.
[41] Ellenbogen T, Seo K, Crozier KB. Chromatic plasmonic polarizers for active visible color filtering and polarimetry. Nano Lett 2012;12:1026–31.
[42] Song M, Li X, Pu M, et al. Color display and encryption with a plasmonic polarizing metamirror. Nanophotonics 2018;7:323–31.
[43] Uddin MJ, Khaleque T, Magnusson R. Guided-mode resonant polarization-controlled tunable color filters. Opt Express 2014;22:12307–15.
[44] Fountaine KT, Whitney WS, Atwater HA. Resonant absorption in semiconductor nanowires and nanowire arrays: Relating leaky waveguide modes to Bloch photonic crystal modes. J Appl Phys 2014;116:153106.
[45] Cao L, Fan P, Barnard ES, Brown AM, Brongersma ML. Tuning the Color of Silicon Nanostructures. Nano Lett 2010;10:2649–54.
[46] Brongersma ML, Cui Y, Fan S. Light management for photovoltaics using high-index nanostructures. Nat Mater 2014;13:451.
[47] Nagasaki Y, Hotta I, Suzuki M, Takahara J. Metal-masked Mie-resonant full-color printing for achieving free-space resolution limit. ACS Photonics 2018;5:3849–55.
[48] Palik ED. Handbook of optical constants of solids. Boston: Academic Press, 1985.

Supplementary Material: The online version of this article offers supplementary material (https://doi.org/10.1515/nanoph-2019-0500).